CHEMISTRY OF MATERIALS
Article

Chem. Mater. **2009,** *21,* 4811–4823 4811
DOI:10.1021/cm901509t

Multifunctional Roles of TiO_2 Nanoparticles for Architecture of Complex Core−Shells and Hollow Spheres of SiO_2−TiO_2−Polyaniline System

Dan Ping Wang and Hua Chun Zeng*

Department of Chemical and Biomolecular Engineering, KAUST-NUS GCR Program, and Minerals, Metals, and Materials Technology Center, Faculty of Engineering, National University of Singapore, 10 Kent Ridge Crescent, Singapore 119260

Received June 2, 2009. Revised Manuscript Received August 25, 2009

Nanoparticles are often used as seeds to grow one-dimensional nanomaterials or as core materials to prepare core−shell nanostructures. On the other hand, the presynthesized inorganic nanoparticles can also be used as starting building blocks to prepare inorganic−polymer nanocomposites. In this work, we explore the roles of metal-oxide nanoparticles (anatase TiO_2) in the area of constructional synthesis of highly complex core−shell and hollow sphere nanostructures comprising SiO_2, TiO_2, and polyaniline (PAN). In particular, multifunctional roles of oleate-surfactant-protected TiO_2 nanoparticles have been revealed in this study: they provide starting sites for polymerization of aniline on the surface of SiO_2 mesospheres; they land on the inner surface of polyaniline shell to form a secondary material phase; they work as initial crystalline seeds for homogeneous growth of interior TiO_2 shell; and they serve as primary nanobuilding blocks to form exterior TiO_2 shell on the polyaniline via self-assembly. With the assistance of the TiO_2 nanoparticles, a total of six complex core−shell and hollow sphere nanocomposites (SiO_2/TiO_2, SiO_2/TiO_2/PAN, SiO_2/TiO_2/PAN/TiO_2, TiO_2/PAN, TiO_2/PAN/TiO_2, and TiO_2/TiO_2) have been made in this work through controlled self-assembly, templating growth, polymerization, and homogeneous seeded growth. Applicability of these nanostructures in photocatalytic applications has also been demonstrated by our preliminary investigations. The easy separation of used catalysts after reaction seems to be advantageous because of relatively large external diameters of the lightweight nanocomposites.

1. Introduction

Over the past 15 years or so, structural and compositional architecture of core−shell materials has received significant research attention,[1−37] because of their importance to the development of nanotechnology in the

*Corresponding author. Tel: (65) 6516-2896. Fax: (65) 6779-1936. E-mail: chezhc@nus.edu.sg.

(1) Schärtl, W. *Adv. Mater.* **2000**, *12*, 1899–1908.
(2) Pastoriza-Santos, I.; Koktysh, D. S.; Mamedov, A. A.; Giersig, M.; Kotov, N. A.; Liz-Marzán, L. M. *Langmuir* **2000**, *16*, 2731–2735.
(3) Zhong, C. J.; Maye, M. M. *Adv. Mater.* **2001**, *13*, 1507–1511.
(4) Hanprasopwattana, A.; Srinivasan, S.; Sault, A. G.; Datye, A. K. *Langmuir* **1996**, *12*, 3173–3179.
(5) Guo, C.-W.; Cao, Y.; Xie, S.-H.; Dai, W.-L.; Fan, K.-N. *Chem. Commun.* **2003**, 700–701.
(6) Sobal, N. S.; Ebels, U.; Möhwald, H.; Giersig, M. *J. Phys. Chem. B* **2003**, *107*, 7351–7354.
(7) Guo, H.-X.; Zhao, X.-P.; Ning, G.-H.; Liu, G.-Q. *Langmuir* **2003**, *19*, 4884–4888.
(8) Lu, Y.; McLellan, J.; Xia, Y. N. *Langmuir* **2004**, *20*, 3464–3470.
(9) Hao, L.-Y.; Zhu, C.-L.; Jiang, W.-Q.; Chen, C.-N.; Hu, Y.; Chen, Z.-Y. *J. Mater. Chem.* **2004**, *14*, 2929–2934.
(10) Zhang, K.; Zhang, X. H.; Chen, H. T.; Chen, X.; Zheng, L. L.; Zhang, J. H.; Yang, B. *Langmuir* **2004**, *20*, 11312–11314.
(11) Yang, H. G.; Zeng, H. C. *Angew. Chem., Int. Ed.* **2004**, *43*, 5206–5209.
(12) Li, J.; Zeng, H. C. *Angew. Chem., Int. Ed.* **2005**, *44*, 4342–4345.
(13) Zhang, Y. X.; Li, G. H.; Wu, Y. C.; Luo, Y. Y.; Zhang, L. D. *J. Phys. Chem. B* **2005**, *109*, 5478–5481.
(14) Li, J.; Zeng, H. C. *Chem. Mater.* **2006**, *18*, 4270–4277.
(15) Li, H. X.; Bian, Z. F.; Zhu, J.; Zhang, D. Q.; Li, G. S.; Hou, Y. N.; Li, H.; Lu, Y. F. *J. Am. Chem. Soc.* **2007**, *129*, 8406–8407.
(16) Lattuada, M.; Hatton, T. A. *J. Am. Chem. Soc.* **2007**, *129*, 12878–12889.
(17) Piao, Y. Z.; Burns, A.; Kim, J. Y.; Wiesner, U.; Hyeon, T. *Adv. Funct. Mater.* **2008**, *18*, 3745–3758.
(18) Zhang, T. R.; Ge, J. P.; Hu, Y. X.; Zhang, Q.; Aloni, S.; Yin, Y. D. *Angew. Chem., Int. Ed.* **2008**, *47*, 5806–5811.
(19) Liu, Y. G.; Feng, X. M.; Shen, J. M.; Zhu, J.-J.; Hou, W. H. *J. Phys. Chem. B* **2008**, *112*, 9237–9242.
(20) Xu, S. P.; Hartvickson, S.; Zhao, J. X. J. *Langmuir* **2008**, *24*, 7492–7499.
(21) Wang, S.; Wang, T.; Chen, W. X.; Hori, T. R. *Chem. Commun.* **2008**, 3756–3758.
(22) Liu, G. Y.; Ji, H. F.; Yang, X. L.; Wang, Y. M. *Langmuir* **2008**, *24*, 1019–1025.
(23) Zhang, H.; Zhong, X.; Xu, J.-J.; Chen, H.-Y. *Langmuir* **2008**, *24*, 13748–13752.
(24) Xuan, S. H.; Wang, Y.-X. J.; Leung, K. C.-F.; Shu, K. Y. *J. Phys. Chem. C* **2008**, *112*, 18804–18809.
(25) Joo, S. H.; Park, J. Y.; Tsung, C.-K.; Yamada, Y.; Yang, P. D.; Somorjai, G. A. *Nat. Mater.* **2009**, *8*, 126–131.
(26) Manna, L.; Scher, E. C.; Li, L. S.; Alivisatos, A. P. *J. Am. Chem. Soc.* **2002**, *124*, 7136–7145.
(27) Talapin, D. V.; Nelson, J. H.; Shevchenko, E. V.; Aloni, S.; Sadtler, B.; Alivisatos, A. P. *Nano Lett.* **2007**, *7*, 2951–2959.
(28) Schrier, J.; Demchenko, D. O.; Wang, L.-W.; Alivisatos, A. P. *Nano Lett.* **2007**, *7*, 2377–2382.
(29) Caruso, F.; Caruso, R. A.; Möhwald, H. *Science* **1998**, *282*, 1111–1114.
(30) Caruso, F. *Adv. Mater.* **2001**, *13*, 11–22.
(31) Caruso, F.; Spasova, M.; Susha, A.; Giersig, M.; Caruso, R. A. *Chem. Mater.* **2001**, *13*, 109–116.
(32) Caruso, R. A.; Susha, A.; Caruso, F. *Chem. Mater.* **2001**, *13*, 400–409.
(33) Liang, Z. J.; Susha, A.; Caruso, F. *Chem. Mater.* **2003**, *15*, 3176–3183.
(34) Park, M.-K.; Onishi, K.; Locklin, J.; Caruso, F.; Advincula, R. C. *Langmuir* **2003**, *19*, 8550–8554.
(35) Khopade, A. J.; Caruso, F. *Chem. Mater.* **2004**, *16*, 2107–2112.
(36) Correa-Duarte, M. A.; Kosiorek, A.; Kandulski, W.; Giersig, M.; Liz-Marzán, L. M. *Chem. Mater.* **2005**, *17*, 3268–3272.
(37) Zhu, Y. F.; Shi, J. L.; Shen, W. H.; Dong, X. P.; Feng, J. W.; Ruan, M. L.; Li, Y. S. *Angew. Chem., Int. Ed.* **2005**, *44*, 5083–5087.

Published on Web 09/22/2009

areas of energy storage systems, drug delivery carriers, composite catalysts, photonic crystals, plasmonics derives, magnetic imaging agents, low κ-dielectrics, chemical and optical sensors, and protected functional materials.[1−37] There have been a great number of synthetic strategies in place for this class of novel materials.[1−37] For instance, heteroepitaxial growth has been commonly adopted for fabrication of II−VI semiconductor quantum dots with multiple shells.[26−28] Because basic crystallographic structures of these compound semiconductors are similar, multiple-shelled nanostructures can be integrated facially via alternating chemical constituents in precursor solutions.[26−28] Another common synthetic route to fabricate core−shells is layer-by-layer (LbL) approach, in which charged polyelectrolytes are first introduced to core supports (e.g., silica or polystyrene beads), followed by deposition of desired coating chemicals or nanoparticles carrying opposite surface charges.[29−37] In this way, the chemical composition and shell thickness can be controlled by the number of process cycles applied, and more robust shell structures can be obtained after shell formation treatments such as additional thermal conversion and/or chemical modifications.[29−37] Furthermore, solution-based synthesis, interfacial crystal growth, polymerization, and direct nanoparticle deposition on different hard templates are prevailing approaches to fabrication of core−shell structures; numerous pathways and deposition routes have been reported over the past decade.[1−25]

Closely related to the above research, hollow structures can be further obtained from the core−shell materials when their central solid cores are removed.[38−56] Because most of core−shell precursors have a spherical geometry, the resultant shell structures normally retain their pristine shape (i.e., hollow spheres).[38−56] Direct preparation of shelled nanostructures can also be achieved without the step of core removal.[57−63] Using various soft templates such as micelles, vesicles, solution inhomogeneities, and even gas bubbles, researchers have prepared different inorganic hollow spheres,[57−63] although uniform size distribution remains as a drawback in this kind of syntheses. It is important to mention that reactive templates or template-free approaches have also gained significant research attention over the past few years.[64−71] In particular, redox replacement reactions and Kirkendall-type diffusions are two important chemical methods for shell-structural formation as well as for compositional tailoring.[64−71] On the other hand, physical processes such as Ostwald ripening and oriented attachment have also been proven to be feasible to generate hollow structures.[72−82] The latter two processes involve solid evacuation of central materials of aggregates and three-dimensional integration of preformed nanocrystals according to their common crystallographic orientations, respectively.[72−82]

Although core−shell materials have been prepared into various complex forms,[1−37] the shells in hollow structures remain relatively simple at the present stage of research.[38−63] In fact, most of them are just mono- or bicomponent.[83−85] Though the research interest in double-shelled or multishelled structures has increased,[86−91]

(38) Göltner, C. G. *Angew. Chem., Int. Ed.* **1999**, *38*, 3155–3156.
(39) Zhong, Z. Y.; Yin, Y. D.; Gates, B.; Xia, Y. N. *Adv. Mater.* **2000**, *12*, 206–209.
(40) Imhof, A. *Langmuir* **2001**, *17*, 3579–3585.
(41) Kim, S.-W.; Kim, M.; Lee, W. Y.; Hyeon, T. *J. Am. Chem. Soc.* **2002**, *124*, 7642–7643.
(42) Aguirre, C. M.; Kaspar, T. R.; Radloff, C.; Halas, N. J. *Nano Lett.* **2003**, *3*, 1707–1711.
(43) Dong, A. G.; Ren, N.; Tang, Y.; Wang, Y. J.; Zhang, Y. H.; Hua, W. M.; Gao, Z. *J. Am. Chem. Soc.* **2003**, *125*, 4976–4977.
(44) Dong, A. G.; Ren, N.; Yang, W. L.; Wang, Y. J.; Zhang, Y. H.; Wang, D. J.; Hu, J. H.; Gao, Z.; Tang, Y. *Adv. Funct. Mater.* **2003**, *13*, 943–948.
(45) Zhu, J.-J.; Xu, S.; Wang, H.; Zhu, J.-M.; Chen, H.-Y. *Adv. Mater.* **2003**, *15*, 156–159.
(46) Yang, Z. Z.; Niu, Z. W.; Lu, Y. F.; Hu, Z. B.; Han, C. C. *Angew. Chem., Int. Ed.* **2003**, *42*, 1943–1945.
(47) Niu, Z. W.; Yang, Z. Z.; Hu, Z. B.; Lu, Y. F.; Han, C. C. *Adv. Funct. Mater.* **2003**, *13*, 949–954.
(48) Xu, X. L.; Asher, S. A. *J. Am. Chem. Soc.* **2004**, *126*, 7940–7945.
(49) Pan, Y.; Huo, K. F.; Hu, Y. M.; Fu, J. J.; Lu, Y. N.; Dai, Z. D.; Hu, Z.; Chen, Y. *Small* **2005**, *1*, 1199–1203.
(50) Dhas, N. A.; Suslick, K. S. *J. Am. Chem. Soc.* **2005**, *127*, 2368–2369.
(51) Teo, J. J.; Chang, Y.; Zeng, H. C. *Langmuir* **2006**, *22*, 7369–7377.
(52) Guan, G. J.; Zhang, Z. P.; Wang, Z. Y.; Liu, B. H.; Gao, D. M.; Xie, C. G. *Adv. Mater.* **2007**, *19*, 2370–2374.
(53) Wang, H. R.; Song, Y. J.; Wang, Z. C.; Medforth, C. J.; Miller, J. E.; Evans, L.; Li, P.; Shelnutt, J. A. *Chem. Mater.* **2008**, *20*, 7434–7439.
(54) Guan, M. Y.; Tao, F. F.; Sun, J. H.; Xu, Z. *Langmuir* **2008**, *24*, 8280–8283.
(55) Zou, H.; Wu, S. S.; Ran, Q. P.; Shen, J. *J. Phys. Chem. C* **2008**, *112*, 11623–11629.
(56) Liu, X. H.; Wu, H. Y.; Ren, F. L.; Qiu, G. Z.; Tang, M. T. *Mater. Chem. Phys.* **2008**, *109*, 5–9.
(57) Collins, A. M.; Spickermann, C.; Mann, S. *J. Mater. Chem.* **2003**, *13*, 1112–1114.
(58) Peng, Q.; Dong, Y. J.; Li, Y. D. *Angew. Chem., Int. Ed.* **2003**, *42*, 3027–3030.
(59) Nakashima, T.; Kimizuka, N. *J. Am. Chem. Soc.* **2003**, *125*, 6386–6387.
(60) Bao, J. C.; Liang, Y. Y.; Xu, Z.; Si, L. *Adv. Mater.* **2003**, *15*, 1832–1835.
(61) Tarimala, S.; Dai, L. L. *Langmuir* **2004**, *20*, 3492–3494.
(62) Hu, J.-S.; Guo, Y.-G.; Liang, H.-P.; Wan, L. J.; Bai, C. L.; Yang, Y.-G. *J. Phys. Chem. B* **2004**, *108*, 9734–9738.
(63) Binks, B. P.; Clint, J. H.; Mackenzie, G.; Simcock, C.; Whitby, C. P. *Langmuir* **2005**, *21*, 8161–8167.
(64) Sun, Y. G.; Xia, Y. N. *Science* **2002**, *298*, 2176–2179.
(65) Goldberger, J.; He, R. R.; Zhang, Y. F.; Lee, S. K.; Yan, H. Q.; Choi, H.-J.; Yang, P. D. *Nature* **2003**, *422*, 599–602.
(66) Sun, Y. G.; Xia, Y. N. *Adv. Mater.* **2004**, *16*, 264–268.
(67) Kirkendall, E.; Thomassen, L.; Upthegrove, C. *Trans. AIME* **1939**, *133*, 186–203.
(68) Kirkendall, E. O. *Trans. AIME* **1942**, *147*, 104–110.
(69) Smigelskas, A. D.; Kirkendall, E. O. *Trans. AIME* **1947**, *171*, 130–142.
(70) Yin, Y.; Rioux, R. M.; Erdonmez, C. K.; Hughes, S.; Somorjai, G. A.; Alivisatos, A. P. *Science* **2004**, *304*, 711–714.
(71) Liu, B.; Zeng, H. C. *J. Am. Chem. Soc.* **2004**, *126*, 16744–16746.
(72) Ostwald, W. *Z. Phys. Chem.* **1900**, *34*, 495–503.
(73) Yang, H. G.; Zeng, H. C. *J. Phys. Chem. B* **2004**, *108*, 3492–3495.
(74) Chang, Y.; Teo, J. J.; Zeng, H. C. *Langmuir* **2005**, *21*, 1074–1079.
(75) Liu, B.; Zeng, H. C. *Small* **2005**, *1*, 566–571.
(76) Zeng, H. C. *J. Mater. Chem.* **2006**, *16*, 649–662.
(77) Li, J.; Zeng, H. C. *J. Am. Chem. Soc.* **2007**, *129*, 15839–15847.
(78) Penn, R. L.; Banfield, J. F. *Am. Mineral.* **1998**, *83*, 1077–1082.
(79) Penn, R. L.; Banfield, J. F. *Science* **1998**, *281*, 969–971.
(80) Penn, R. L. *J. Phys. Chem. B* **2004**, *108*, 12707–12712.
(81) Yang, H. G.; Zeng, H. C. *Angew. Chem., Int. Ed.* **2004**, *43*, 5930–5933.
(82) Liu, B.; Zeng, H. C. *J. Am. Chem. Soc.* **2004**, *126*, 8124–8125.
(83) Yin, Y. D.; Lu, Y.; Gates, B.; Xia, Y. N. *Chem. Mater.* **2001**, *13*, 1146–1148.
(84) Xuan, S. H.; Jiang, W. Q.; Gong, X. L.; Hu, Y.; Chen, Z. Y. *J. Phys. Chem. C* **2009**, *113*, 553–558.
(85) Zhang, J.; Wang, S. R.; Xu, M. J.; Wang, Y.; Xia, H. J.; Zhang, S. M. *J. Phys. Chem. C* **2009**, *113*, 1662–1665.
(86) Yang, M.; Ma, J.; Zhang, C. L.; Yang, Z. Z.; Lu, Y. F. *Angew. Chem., Int. Ed.* **2005**, *44*, 6727–6730.
(87) Yang, M.; Ma, J.; Niu, Z. W.; Dong, X.; Xu, H. F.; Meng, Z. K.; Jin, Z. G.; Lu, Y. F.; Hu, Z. B.; Yang, Z. Z. *Adv. Funct. Mater.* **2005**, *15*, 1523–1528.
(88) Lou, X. W.; Yuan, C. L.; Archer, L. A. *Small* **2007**, *3*, 261–265.
(89) Xu, H. L.; Wang, W. Z. *Angew. Chem., Int. Ed.* **2007**, *46*, 1489–1492.
(90) Lou, X. W.; Archer, L. A.; Yang, Z. C. *Adv. Mater.* **2008**, *20*, 3987–4019.
(91) Yao, K. X.; Zeng, H. C. *J. Phys. Chem. C* **2009**, *113*, 1373–1385.

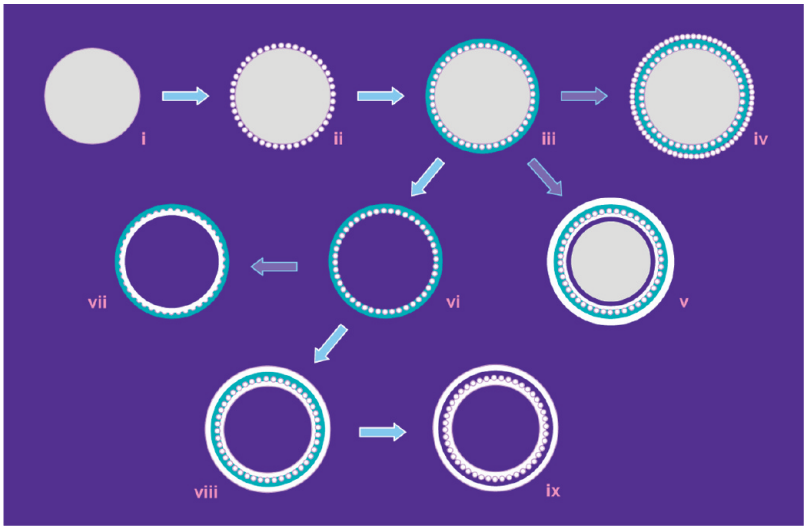

Figure 1. Schematic flowchart (cross-section views) for various nanoparticle-mediated synthetic schemes: (i) as-synthesized SiO_2 sphere, (ii) self-assembly of TiO_2 nanoparticle seeds (tiny white dots) on SiO_2 sphere, (iii) polymerization and formation of polyaniline (PAN, green layer) shell on SiO_2/TiO_2 sphere, (iv) addition of TiO_2 nanoparticles on the PAN shell, (v) growth of TiO_2 on both inner and outer surfaces of TiO_2/PAN shell, (vi) removal of SiO_2 core and formation of TiO_2/PAN hollow sphere, (vii) growth of TiO_2 on the inner surface of TiO_2/PAN hollow sphere, (viii) growth of TiO_2 on both inner and outer surfaces of TiO_2/PAN hollow sphere, and (ix) removal of PAN middle layer and formation of double-shelled TiO_2 hollow sphere.

controllability of complex shell structures remains to be low. To meet new challenges imposed by rapid development of nanotechnology, from a fundamental viewpoint, it would be highly desirable to explore new architectural concepts and processes for fabricating core−shell as well as hollow nanostructures that possess structurally and compositionally complex shells.[76] In pursuing this research, we note that nanoparticles are often used as seeds to grow one-dimensional nanomaterials or as core materials to prepare core−shell nanostructures.[92] On the other hand, these presynthesized inorganic nanoparticles can also be used as starting building blocks to prepare inorganic-polymer nanocomposites.[93] In this contribution, we explore the roles of metal-oxide nanoparticles in the constructional synthesis of complex nanostructures of core−shells and hollow spheres. Our study indicates that this nanoparticle-mediated approach has high synthetic flexibility for core−shell and hollow sphere architectures. Briefly, the main steps of this approach involve synthesis of monodisperse core templates, installation of inorganic seeds, deposition of organic phase, growth and/or formation of inner or outer inorganic shells. As illustrated in Figure 1, self-assembled oleate-surfactant capped TiO_2 nanoparticles serve both as starting points for the deposition of polyaniline shell and as nucleation sites for the seeded growth of TiO_2 inner shell. On the other hand, the same TiO_2 nanoparticles form a secondary material phase imbedded in the inner surface of polyaniline shell and act as building blocks for the formation of external TiO_2 shell via self-assembly. When silica cores or polyaniline shells are removed, a variety of final products can be further fabricated. Because main process steps involved in this approach are well separate and relatively simple (such as self-assembly, templating growth, polymerization, and homogeneous seeded growth, etc.), we believe that the current architectural design and synthetic approach can be easily extended to other complex polymer−metal-oxide systems.

2. Experimental Section

2.1. Synthesis of SiO_2 Mesospheres. SiO_2 mesospheres were prepared according to a reported process with some modifications.[94,95] Briefly, 1.0 mL of tetraethyl orthosilicate (TEOS, Fluka, ≥99%) was first dissolved in a mixture of 18.4 mL of ethanol and 4.5 mL of deionized water in a 100 mL glass bottle. Afterward, 25.0 mL of ammonia solution (28%) was added dropwise to the above solution under vigorous magnetic stirring within 10 min. During the addition of ammonia, the clear solution turned to white gradually. The hydrolysis of TEOS and related condensation reactions lasted for another 4 h with the same magnetic stirring. The SiO_2 mesospheres (Figure 1(i)) were washed with ethanol and deionized water thoroughly and dried in an electric oven at 70 °C overnight.

2.2. Synthesis of TiO_2 Nanoparticles. Monodisperse TiO_2 nanoparticles (TiO_2 NPs) was prepared according to a reported process with minor modifications.[96,97] Briefly, 0.10 mL of tert-butylamine (Aldrich, 98% (GC)) was added to 10.0 mL of deionized water. Meanwhile, 0.15 g of Ti-*n*-propoxide (98%, Alfa Aesar) and 6.0 mL of oleic acid (OA, $CH_3(CH_2)_7$-$CH{=}CH(CH_2)_7COOH$, 90−95%, Alfa Aesar) were added into 10.0 mL of toluene (or cyclohexane). The above two phases were then mixed and transferred to a Teflon-lined stainless steel autoclave. Hydrothermal synthesis was conducted at 180 °C for 4 h in an electric oven. When the reaction

(92) Barrelet, C. J.; Wu, Y.; Bell, D. C.; Lieber, C. M. *J. Am. Chem. Soc.* **2003**, *125*, 11498–11499.
(93) Wang, D. P.; Zeng, H. C. *J. Phys. Chem. C* **2009**, *113*, 8097–8106.
(94) Stöber, W.; Fink, A.; Bohn, E. *J. Colloid Interface Sci.* **1968**, *26*, 62–69.
(95) Rao, K. S.; El-Hami, K.; Kodaki, T.; Matsushige, K.; Makino, K. *J. Colloid Interface Sci.* **2005**, *289*, 125–131.
(96) Pan, D.; Zhao, N.; Wang, Q.; Jiang, S.; Ji, X.; An, L. *Adv. Mater.* **2005**, *17*, 1991–1995.
(97) Li, J.; Tang, S. B.; Lu, L.; Zeng, H. C. *J. Am. Chem. Soc.* **2007**, *129*, 9401–9409.

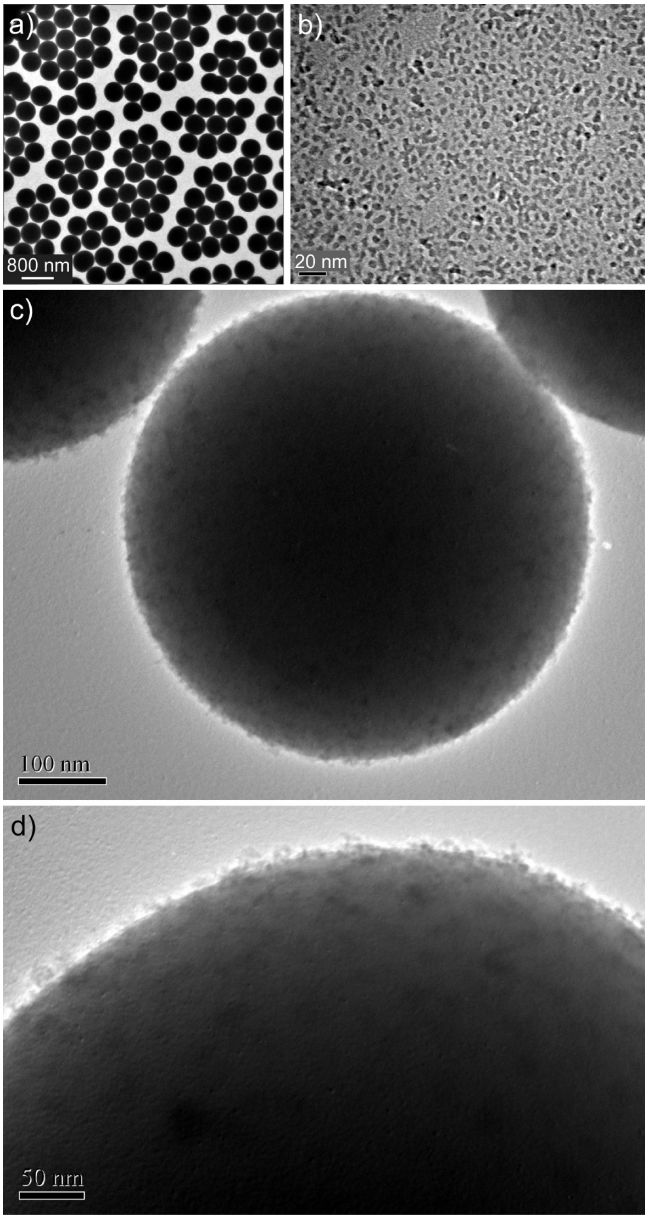

Figure 2. TEM images: (a) as-prepared SiO_2 spheres, (b) free-standing TiO_2 nanoparticles (seeds), (c) self-assembly of TiO_2 nanoparticle seeds on SiO_2 spheres, and (d) a detailed view of TiO_2 nanoparticle seeds on SiO_2 spheres.

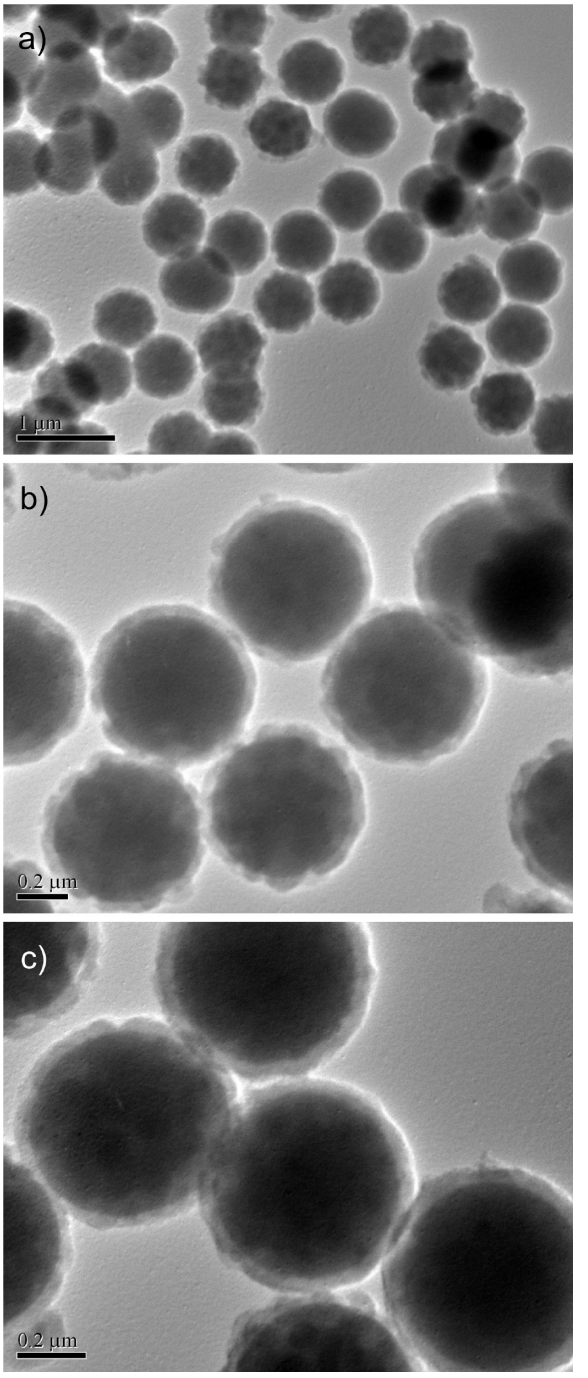

Figure 3. TEM images of as-prepared SiO_2/TiO_2/PAN spheres at different magnifications.

was completed, the organic phase was extracted and added in an equal volume of methanol to sedimentate TiO_2 NPs. After centrifuging, methanol was removed and TiO_2 NPs were redispersed into 8.0 mL of toluene (or cyclohexane); the concentration of TiO_2 NPs in the thus prepared suspension was 3.5 mg/mL.

2.3. Synthesis of SiO_2/TiO_2 via Self-Assembly. An amount of 40.0 mg of the above prepared SiO_2 spheres was first dispersed into 2.0 mL of toluene in an ultrasonic water bath for 20 min. Afterward, 1.0 mL of the TiO_2 NPs suspension (in toluene) was added, the mixture was continuously sonicated for another 1−2 h. The resultant SiO_2/TiO_2 (Figure 1(ii)) product was washed with toluene once and dried at 70 °C in an electric oven overnight.

2.4. Synthesis of SiO_2/TiO_2/PAN. An amount of 20.0 mg of the as-prepared SiO_2/TiO_2 spheres was first dispersed in 30.0 mL of ethanol in an ultrasonic water bath for 5 min. Ethanol phase remained to be clear after dispersing SiO_2/TiO_2 spherical particles. Then, 0.05 mL of aniline (the monomer for polyaniline (PAN); the actual concentration of aniline before polymerization was 0.018 M) was added into the solution, and followed by another 5 min sonication to have the monomers fully dispersed in ethanol. Afterward, 1.0 mL of HCl aqueous solution (1.21 M) which contained 0.156 g of ammonium peroxydisulfate $(NH_4)_2S_2O_8$ (APS, $(NH_4)_2S_2O_8$, Alfa Aesar, 98%) was added into the above ethanol phase. The solid−solution mixture was sonicated continuously for another 4 h in an ultrasonic water bath during which the PAN shell was formed. The dark green product (Figure 1(iii)) was washed with ethanol and deionized water several times and stored in ethanol. Dynamic investigation of this reaction

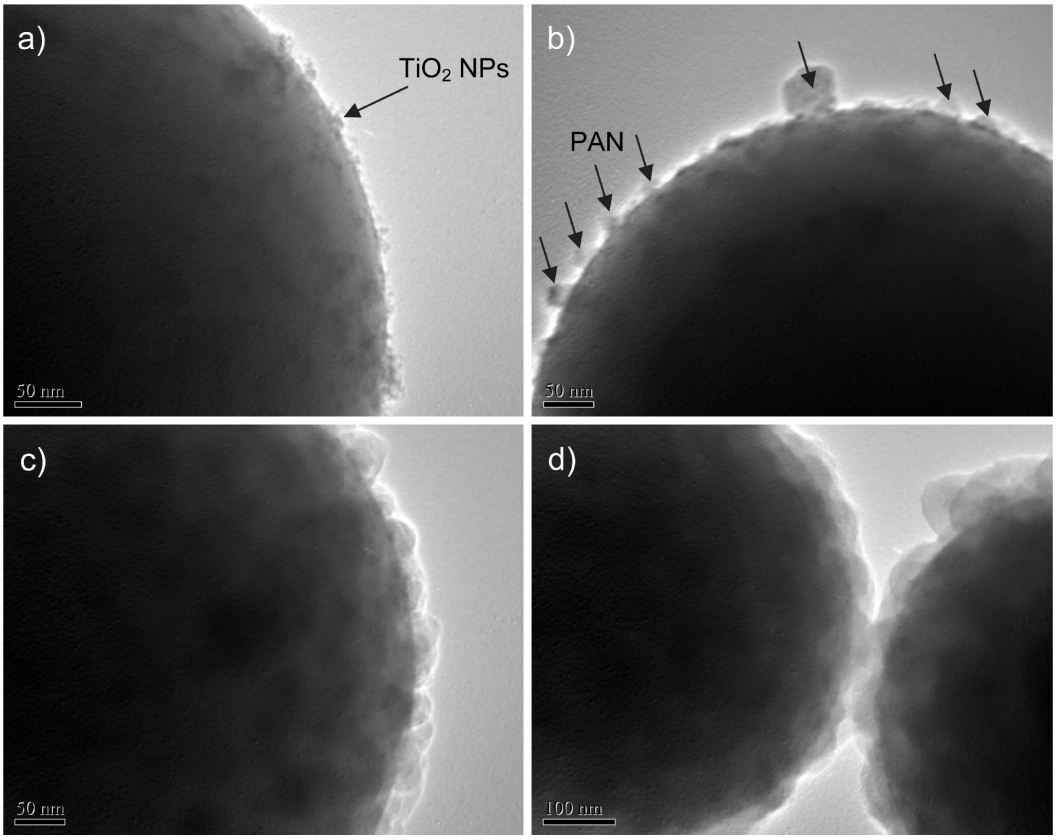

Figure 4. TEM images of deposition process of polyaniline (PAN) on the spheres of SiO_2/TiO_2 at different times: (a) before polymerization (0 min; i.e., SiO_2/TiO_2), (b) 20 min, (c) 40 min, and (d) 60 min after reactions.

process was also carried out and the intermediate products were collected at 20 min, 40 min, 1 h, 2 h, and 4 h after the polymerization.

2.5. Synthesis of $SiO_2/TiO_2/PAN/TiO_2$. In this preparation, 2.0 mL of $SiO_2/TiO_2/PAN$ (10.0 mg of $SiO_2/TiO_2/PAN$) ethanol suspension was added into a mixture of 10.0−20.0 mL of ethanol, 4.0−14.0 mL of deionized water, and 1.0−6.0 mL of 0.040 M TiF_4 solution.[98] The mixture was sonicated for 10 min, and later transferred into a water-bath tank at 70 °C. The whole reaction lasted for 4 h with magnetic stirring. The $SiO_2/TiO_2/PAN/TiO_2$ products (Figure 1(v)) were washed with ethanol and deionized water, and stored in ethanol for materials characterization. Alternatively, the outmost TiO_2 layer could also be added onto $SiO_2/TiO_2/PAN$ by self-assembly method. For example, 20.0 mg of dried $SiO_2/TiO_2/PAN$ powder was dispersed in 2.0 mL of toluene under sonication conditions. After 20 min, 1.0 mL of TiO_2 NPs suspension (in toluene) was added, followed by 2 h sonication. The thus prepared $SiO_2/TiO_2/PAN/TiO_2$ sample (Figure 1(iv)) was washed with toluene and dried at 60 °C in an electric oven overnight.

2.6. Preparation of Hollow TiO_2/PAN. First, 4.0 mL of the above prepared $SiO_2/TiO_2/PAN$ ethanol suspension which contained around 40.0 mg of solid powder was added into 5.0 mL of ethanol. The suspension was then sonicated for 5 min in order to make the particles evenly distributed in ethanol, followed by addition of 1.0 mL of 49.0% HF solution (Note: total solution volume now was ca. 10 mL). The etching process for SiO_2 cores was carried out for 10 min. The above prepared TiO_2/PAN hollow spheres (Figure 1(vi)) were washed with deionized water 3 times. The collected powder was then dried in a vacuum oven at 50 °C for 2 h.

2.7. Preparation of Hollow $TiO_2/PAN/TiO_2$. The growth of TiO_2 on the shell of TiO_2/PAN hollow spheres was carried out at 70 °C in a water bath and at 180 °C under hydrothermal condition respectively (Figure 1(vii) and 1(viii)). For water bath synthesis, 4.0 mg of TiO_2/PAN hollow spheres was dispersed into a solution mixture prepared from 20.0 mL of ethanol, 2.0−4.0 mL of deionized water and 6.0−8.0 mL of 0.04 M TiF_4 solution. This solid−solution system was sonicated for 10 min before it was moved into a water bath. Then the reaction was carried out at 70 °C for 4 h with vigorous magnetic stirring. The product sample was washed with ethanol thoroughly. For the hydrothermal reaction, 2.5 mg of TiO_2/PAN hollow spheres was dispersed into a solution mixture of 20.0 mL of ethanol, 2.0−8.0 mL of deionized water, and 2.0−8.0 mL of 0.04 M TiF_4 solution. After being sonicated for 10 min, the solid−solution mixture was transferred to a Teflon-lined stainless steel autoclave. The hydrothermal reaction was carried out at 180 °C for 2 h inside an electric oven.

2.8. Preparation of Hollow TiO_2/TiO_2. The double-shelled TiO_2 hollow spheres were prepared by thermal removal of PAN phase from the above prepared $TiO_2/PAN/TiO_2$. For example, the $TiO_2/PAN/TiO_2$ samples could be heat-treated at 450 °C for 4 h in an electric furnace, during which PAN was completely oxidized into gaseous products with laboratory air, resulting in double-shelled anatase TiO_2 (Figure 1(ix)).

2.9. Photocatalytic Reactivity. In the photocatalytic investigation, a certain amount of powders of $SiO_2/TiO_2/PAN/TiO_2$ core−shells, triple-shelled $TiO_2/PAN/TiO_2$, double-shelled TiO_2/TiO_2 hollow spheres, and Hombikat UV 100 (a commercialized TiO_2 product widely used for photocatalytic activity

(98) Yang, H. G.; Zeng, H. C. *J. Phys. Chem. B* **2003**, *107*, 12244–12255.

comparison) was dispersed, respectively, into 50.0−75.0 mL of methyl orange aqueous solution (10 mg/L) via sonication and the solid in the final suspension had a constant concentration of 0.1 mg/mL; the mixture was then stirred at room temperature for 1−2 h to achieve adsorption equilibrium for methyl orange ($C_{14}H_{14}N_3NaO_3S$). Afterward, the solid−solution mixture was illuminated by a Hg lamp (125 W; Philips) with a cutoff filter (λ = 360 nm) for 15−140 min, during which a volume of 4.0 mL of solution together with the catalyst was drawn out repeatedly at constant time interval in order to determine the concentration of remaining reactant using UV−visible spectrophotometry (Shimadzu UV-2450); the solution used for this measurement was separated from the catalyst by centrifugation.

2.10. Materials Characterization. The crystallographic information of the prepared core−shells and hollow spheres was established by powder X-ray diffraction (XRD, Shimadzu XRD-6000, Cu Kα). The structural and morphological investigations of the samples were carried out with transmission electron microscopy (TEM, JEM-2010) and field emission scanning electron microscopy (FESEM, JSM-6700F). Compositional analysis for the samples was performed with X-ray photoelectron spectroscopy (XPS, AXIS-HSi, Kratos Analytical) and Fourier transform infrared spectroscopy (FTIR, Bio-Rad), respectively. The content of polyaniline in the samples was determined using a thermogravimetric method (TGA, TA Instruments TGA 2050). Surface area and porosity analysis of the nanocomposite was investigated by (BET and BJH methods (NOVA-3000).

3. Results and Discussion

Figure 1 depicts several nanoparticle-mediated synthetic routes for major core−shell nanostructures combined from silica (SiO_2), anatase titania (TiO_2), and polyaniline (PAN) and for a variety of multishelled spherical derivatives prepared in this work. Two types of blocks used for making initial SiO_2/TiO_2 nanocomposites are displayed in Figure 2a-b, respectively. As shown, the as-synthesized silica mesospheres are monodisperse with an average diameter of about 640 nm, and the TiO_2 nanoparticles (TiO_2 NPs), which were used as both a seed material and a surface coating material in this approach, have a narrow size distribution range of 3−6 nm. After deposition of TiO_2 NPs, the surface of SiO_2 mesospheres became rougher (Figure 2c,d and Figure 1(ii)). The major driving force for this self-assembly process could be attributed to the chelating action of deprotonated hydroxyl groups on SiO_2 surface to unprotected Ti^{4+} sites on TiO_2 NPs.[98] Nevertheless, a small degree of aggregation among the TiO_2 NPs is also observed (Figure 2d), in which van der Waals interaction among the surfactant molecules (i.e., oleate−surfactant headgroups on TiO_2) is also present. Hence, the resultant SiO_2/TiO_2 products are free of unsupported TiO_2 NPs.

The above prepared SiO_2/TiO_2 core−shell nanocomposites were then used as template for polyaniline deposition, as illustrated in Figure 1(iii). Arising from this polymerization process, a compact PAN shell can be formed evenly on this core−shell template. In Figure 3,

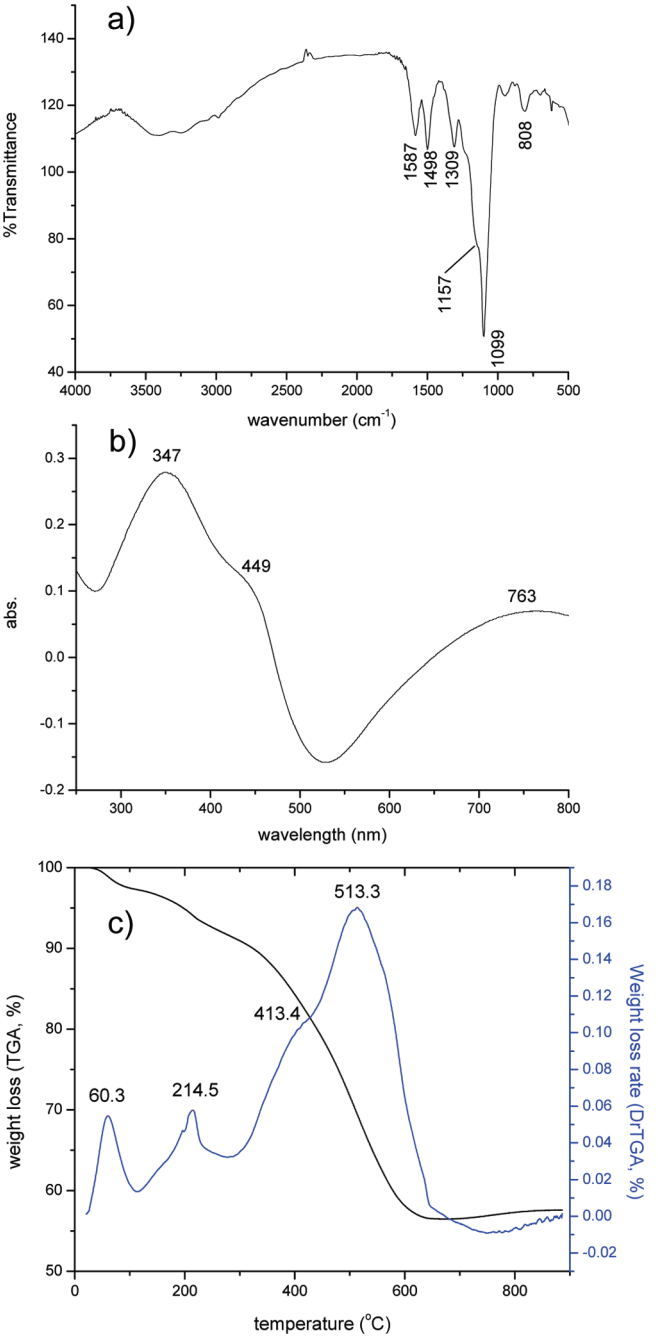

Figure 5. Materials characterization of spheres of SiO_2/TiO_2/PAN: (a) FTIR spectrum, (b) UV−visible absorbance spectrum, and (c) TGA/DrTGA curves.

a representative product of such SiO_2/TiO_2/PAN core−shells (whose shell thickness is *ca* 44 nm) is displayed. In order to have a better understanding of the shell formation, intermediate products at different reaction times were collected sequentially for TEM observation, and a series of TEM images during the polymerization of aniline is reported in Figure 4. At the 20th min (Figure 4b) of reaction, we found that tiny PAN particles with the average diameter of ca. 17.8 nm were formed on the surface of SiO_2/TiO_2. Accordingly, the reacting mixture turned from colorless to blue by eye observation, which indicated that the polymerization had taken place at this time. We found that polyaniline prefers to grow on the

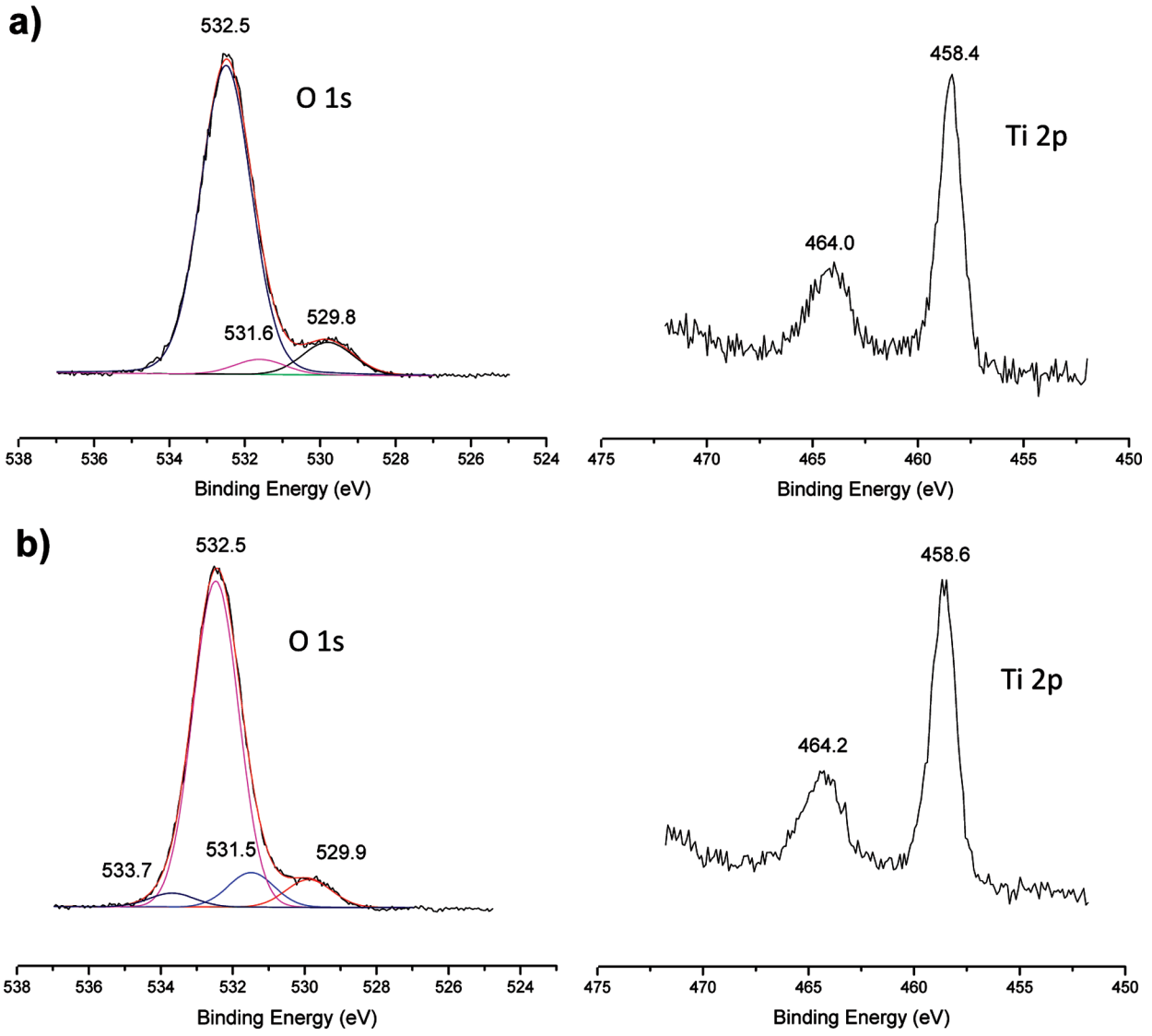

Figure 6. XPS analysis of SiO_2/TiO_2 nanocomposites: (a) as-prepared SiO_2/TiO_2 (Figure 2c,d) and (b) SiO_2/TiO_2 obtained after thermal removal of PAN phase from SiO_2/TiO_2/PAN (i.e., after the TGA analysis in Figure 5c).

SiO_2/TiO_2 core−shell template than to grow as freestanding particles in a separate phase. This observation might be due to the affinity of oleate surfactant headgroups on TiO_2 NPs,[93] whereby aniline monomer anchors on. After the addition of initiator solution (HCl-APS), which was miscible in ethanol phase, polymerization started from the interface of SiO_2/TiO_2 and ethanol. Because of the similar hydrophobic interaction, oleated anatase nanoparticles seemed to provide initial nucleation sites for the formation of polyaniline seed particles. Once the polyaniline seeds were formed on the SiO_2/TiO_2 template, site-selective polymerization would be increased. The average diameter of polyaniline particles increased to 33.4 nm during the first 40 min of the reaction (Figure 4c). Meanwhile, the density of PAN particles became higher with the longer reaction times. After 1 h of the reaction, the individual PAN particles merged when the polymeric particles grew larger (Figure 4d). At this point in time, the PAN shell had a raspberry-like morphology with a thickness of ca. 34.0 nm. The shell became flattened and continued to increase to 44.0 and 44.4 nm after 2 and 4 h (Figure 3) of reactions, respectively. It should be pointed out that the presence of TiO_2 NPs (i.e., seeds) is an important prerequisite for the PAN shell formation, which will be addressed below.

The above prepared SiO_2/TiO_2/PAN was characterized with various analytical techniques. For example, the IR spectrum in Figure 5a shows the characteristic absorptions of polyaniline in the nanocomposites. In particular, the peaks at 1587 and 1498 cm^{-1} can be assigned to the stretching vibrations of quininoid and benzenoid rings, respectively, while the peak at 1309 cm^{-1} and a small shoulder at around 1250 cm^{-1} belong to C−N and protonated C−N stretching modes.[99] The shoulder peak at 1157 cm^{-1} can be assigned to in-plane bending mode of C−H,[99] and the sharp peak at 1099 cm^{-1} to the Si−O−Si stretching band of the SiO_2 cores.[100] In Figure 5b, the UV−vis absorption band at 347 nm is assigned to $\pi-\pi^*$

(99) Mallick, K.; Witcomb, M. J.; Scurrell, M. S. *J. Phys.: Condens. Matter* **2007**, *19*, 196225.
(100) Zhan, Z. Q.; Zeng, H. C. *J. Mater. Chem.* **1999**, *9*, 2647–2652.

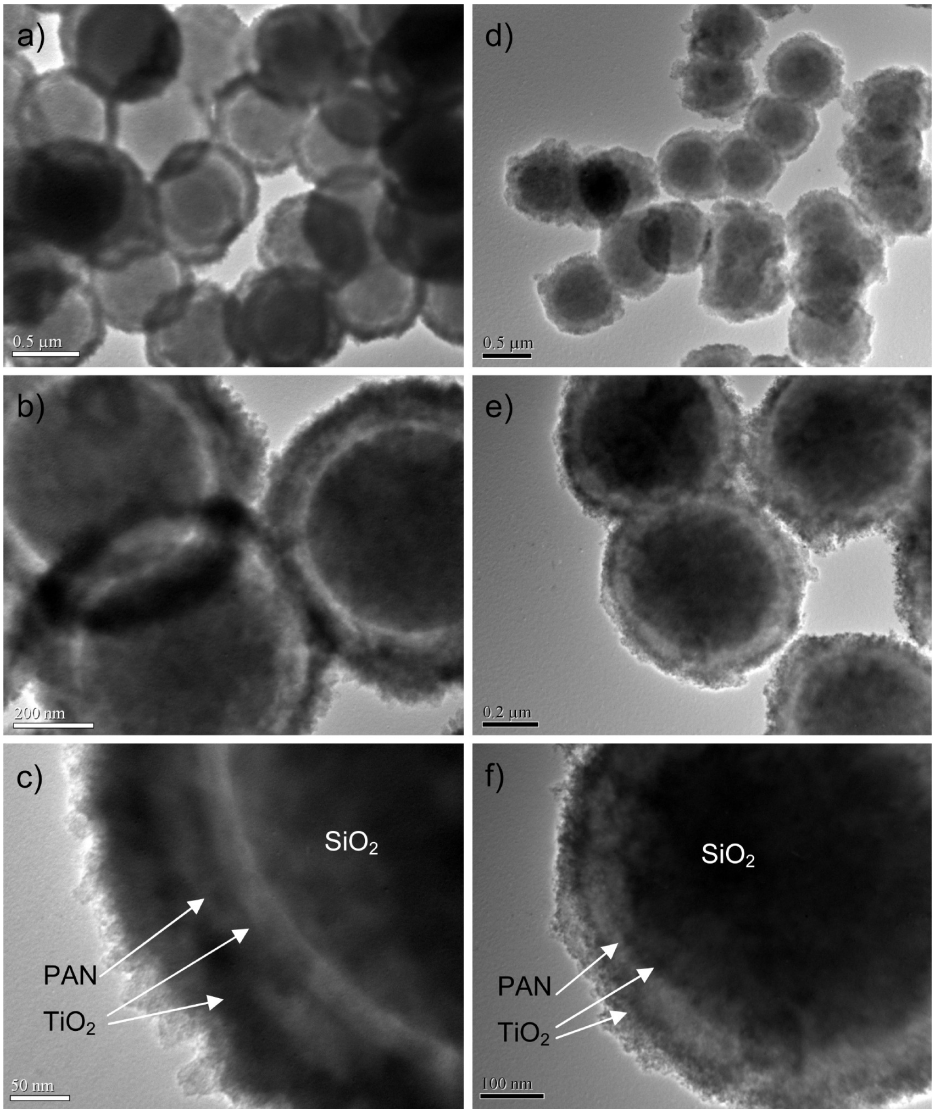

Figure 7. TEM images of two types of $SiO_2/TiO_2/PAN/TiO_2$ core−shells at different magnifications: (a−c) the outmost TiO_2 phase was deposited by growth method, and (e, f) the outmost TiO_2 phase was deposited by self-assembly method.

transition in the benzenoid rings, and the absorptions at 449 and ca. 763 nm are ascribed to polaron−π* transition and polaron−π transition,[101] respectively. The polaron−π transition in the composite sample at ca. 763 nm confirms the formation of doped polyaniline (i.e., emeraldine salt).[101] TGA scan and DrTGA curve in Figure 5c indicate that a PAN loading on the SiO_2/TiO_2 support in this case was about 30 wt %. The first two thermal events at 60.3 and 214.5 °C are attributed to evaporation of water molecules and desorption/decomposition of adsorbed anions inherited from the synthesis (Experimental Section). The major thermal events at 413.4 and 513.3 °C are assigned to the combustion of oleate surfactant (on TiO_2 NPs) and polyaniline, respectively. To confirm the presence of the TiO_2 NPs throughout the polymerization process, we further carried out an XPS investigation. Figure 6a shows the surface composition of the SiO_2/TiO_2 prior to polymerization (Figure 2c,d). In particular, the O 1s peak at 532.5 eV can be assigned to the oxygen in Si−O−Si bonds,[102] and the smaller peak at 529.8 eV to the lattice oxygen in anatase TiO_2,[97] while a tiny component located at 531.6 eV can be attributed to oxygen in surface −OH groups on the SiO_2 cores.[102] In Figure 6b, the peak at 529.9 eV for O 1s and the doublet peaks for Ti 2p indicate that TiO_2 nanoparticle seeds were still on the surface even after removing the PAN shell.[97] The positive binding energy shifts (+0.2 eV) for Ti 2p doublets are due to the formation of Si−O−Ti linkages in this heat-treatment.[103,104] Apparently, the oxide phase became more hydrophilic after removal of organics, because the component located at 531.5 eV became more pronounced and a new component at 533.7 eV (oxygen in water molecules) could now be detected.[97] In other words, SiO_2/TiO_2 surface composite did not break down during ultrasonic polymerization and thus the TiO_2 NPs could serve as starting points for polyaniline to nucleate.

(101) Huang, W. S.; MacDiarmid, A. G. *Polymer* **1993**, *34*, 1833–1845.
(102) Teo, S. H.; Zeng, H. C. *J. Phys. Chem. B* **2001**, *105*, 9093–9100.
(103) Barr, T. L. *J. Vac. Sci. Technol., A* **1991**, *9*, 1793–1805.
(104) Barr, T. L.; Lishka, M. A.; Chen, L. M.; Mohsenian, M. *J. Am. Chem. Soc.* **1988**, *110*, 7962–7975.

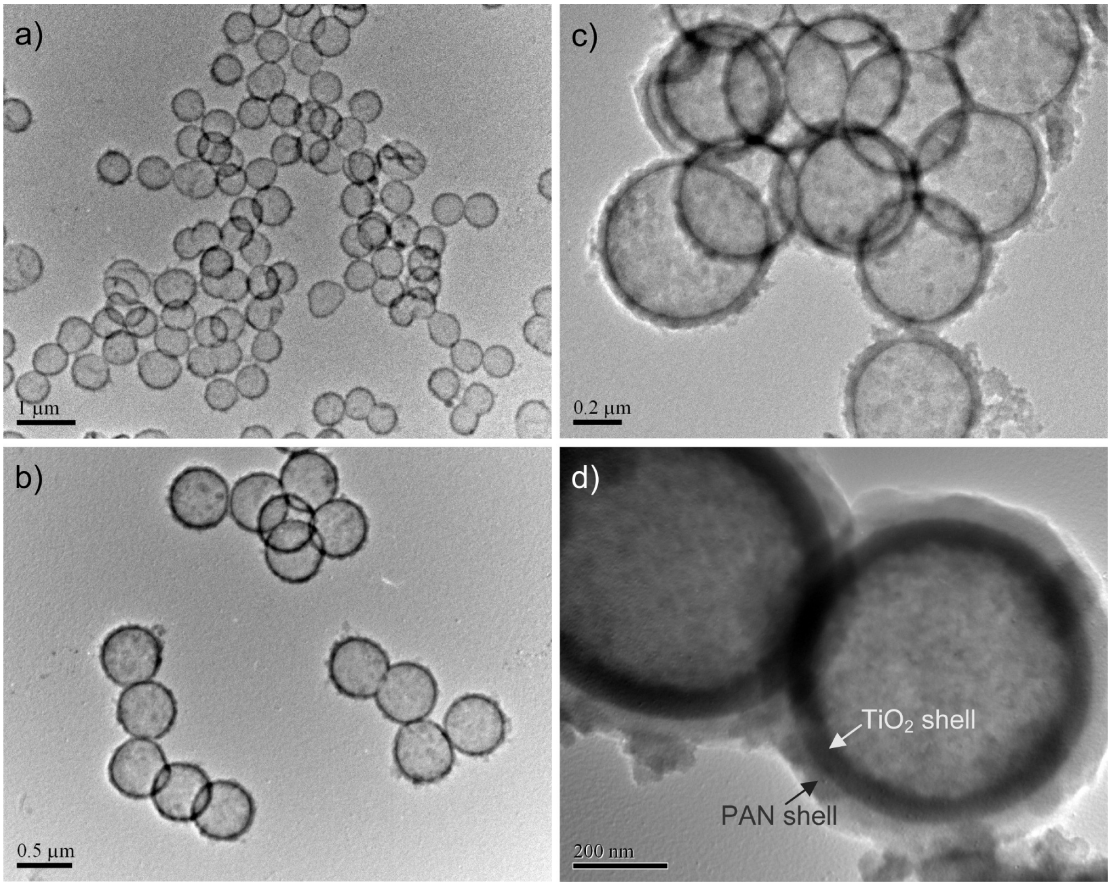

Figure 8. (a−c) TEM images of TiO_2/PAN hollow spheres at different magnifications, noting that a small TiO_2 phase (i.e., TiO_2 NPs (seeds)) is located on the inner surface of the spheres, and (d) TEM image of TiO_2/PAN hollow spheres with a thick inner shell of TiO_2 after a selective growth.

Our TEM investigation also found that TiO_2 NPs were still on the surface after thermal removal of PAN (see the Supporting Information, SI-1), that is, TiO_2 NPs were immobilized on the surface of silica throughout the polymerization process. Furthermore, we also confirmed that these TiO_2 NPs were indeed indispensable for the formation of PAN shell in our synthesis. As a comparison, pristine SiO_2 spheres without any TiO_2 nanoparticles were also used as templates for aniline polymerization. Interestingly, when there were no surface TiO_2 NPs involved in the reactions, large polyaniline petals with an average diameter of ca. 267 nm were found scattered on the silica surface instead of a spherical shell around the surface of SiO_2 mesospheres (see the Supporting Information, SI-2). Apparently, unmodified silica has little chemical affinity to aniline and its polymer, and the growth of PAN is limited to few nucleation sites available, resulting in the petallike morphology.

Many complex core−shell or hollow sphere configurations can be derived from the above prepared SiO_2/TiO_2/PAN precursor (Figure 1(iii)). For example, two types of SiO_2/TiO_2/PAN/TiO_2 core−shells that comprise two shells of TiO_2 and one shell of PAN (Figure 1(iv) and (v)) were prepared in this work. In Figure 7a−c, the outmost anatase TiO_2 shell was deposited by direct hydrolysis of TiF_4. When TiF_4 hydrolyzes at 60−70 °C in aqueous phase, the raspberry-like PAN shell acts as a permeable membrane and allows TiF_4 to penetrate through it. Illustrated in Figure 7c, as a result, TiF_4 hydrolysis takes place on both the outer and inner surfaces of the polymeric shell, giving rise to formation of TiO_2 on their surfaces. This observation will be further addressed in Figure 8. Due to the generation of HF from this reaction, on the other hand, the SiO_2 cores were partially removed, resulting from chemical etching (i.e., HF as an etchant). These two reactions are described in eqs 1 and 2 below[98]

$$TiF_4 + 2H_2O \rightarrow TiO_2 + 4HF \quad (1)$$

$$SiO_2 + 4HF \rightarrow SiF_4 + 2H_2O \quad (2)$$

Note that the second reaction (eq 2) quickly depletes the hydrolysis product (HF) at SiO_2 cores and thus further promotes TiF_4 to hydrolyze on the surfaces of polyaniline. As the reaction goes on, more HF pass through the polyaniline shell to react with SiO_2, and thus the space between the PAN shell and SiO_2 core increases, which can be clearly seen in Figure 7a-c (Figure 1(v)). Through our synthetic investigations (with TiF_4 precursor concentrations: 1.3×10^{-3} to 8.0×10^{-3} M), we also found that TiF_4 prefers to hydrolyze on the polyaniline surfaces and the resultant vacant space between the shell and core is proportional to the TiF_4 concentration used in synthesis. In addition to the direct growth, the external oxide

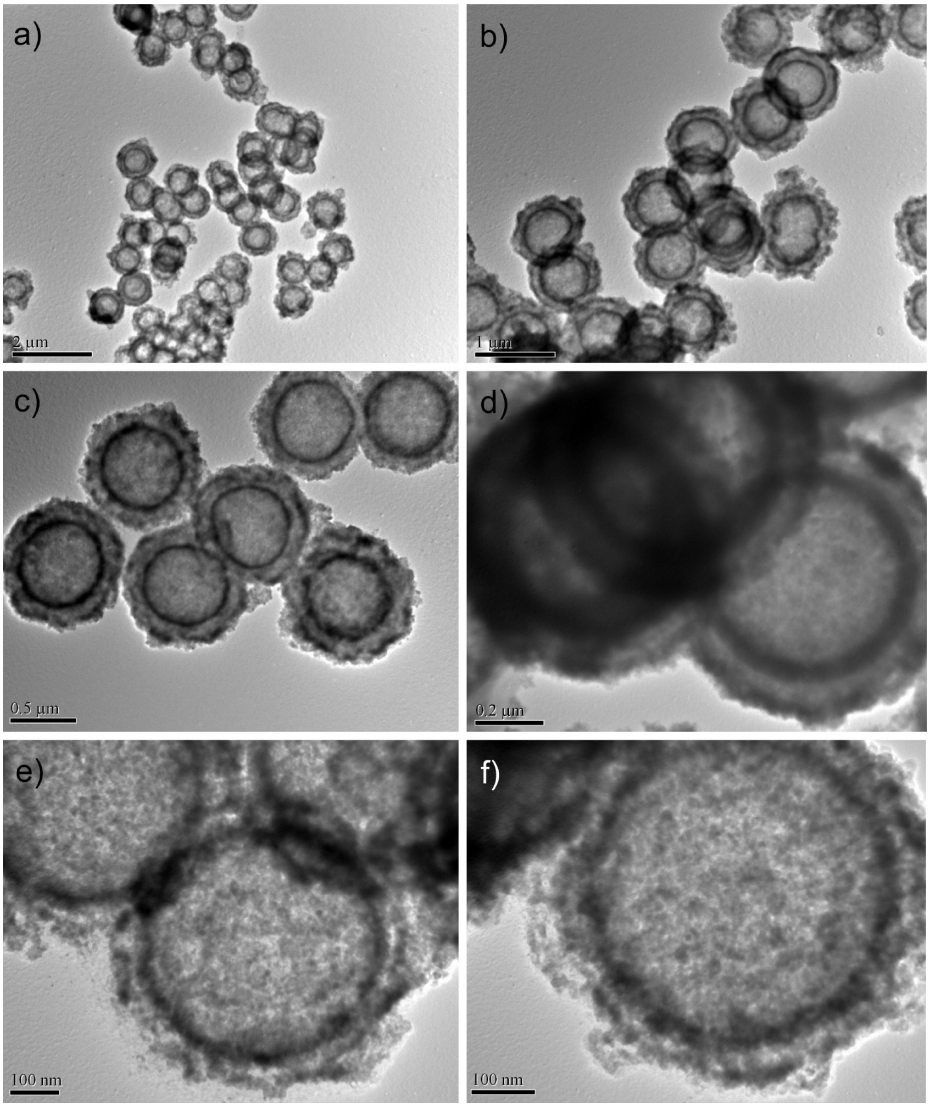

Figure 9. TEM images of two types of multishelled anatase TiO_2 at different magnifications: (a−d) triple-shelled TiO_2/PAN/TiO_2 hollow spheres, and (e, f) double-shelled TiO_2/TiO_2 hollow spheres after removal of PAN interlayer.

surface phase can also be introduced using the presynthesized TiO_2 NPs via self-assembly. In Figure 7d−f, the outmost anatase TiO_2 shell was formed from aggregative TiO_2 NPs on the PAN substrate. As discussed earlier, van der Waals interaction is the major binding force between the polyaniline and oleated anatase nanoparticles in this complex self-assembled core−shell structure (Figure 1(iv)).

In addition to a partial removal, the SiO_2 phase in the SiO_2/TiO_2/PAN and SiO_2/TiO_2/ PAN/TiO_2 core−shells can be completely removed in dilute HF solutions, giving rise to different types of multishelled hollow spheres (Figure 1(vi) to (ix); see the Supporting Information, SI-3). In particular, TiO_2/PAN hollow structure was selected for an in-depth investigation (Figure 1(vi)). Figure 8 shows the TiO_2/PAN hollow spheres prepared by the chemical etching method (eq 2) using the SiO_2/TiO_2/PAN as a precursor. The as-prepared TiO_2/PAN hollow spheres have a mean diameter of ca. 585 nm, and they appear to be fairly robust even after dissolving SiO_2 cores, showing no signs of flattening. Because the interior surface has a thin layer of TiO_2 NPs and the polymerization reaction was taken place on their surfaces, as mentioned earlier, smoother interior surfaces are observed, compared to the exterior surfaces (Figure 8a−c). In this study, these hollow spheres were used as templates for synthesis of double-shelled anatase TiO_2. Though XRD technique was not able to detect pristine anatase TiO_2 NPs (seeds) in the composite, because of its small quantity, the anatase nanoparticles could withstand the HF etchant and they were anchored on the inner surface of polyaniline shell. When the TiO_2/PAN hollow spheres are used as templates, surprisingly,

Table 1. Specific Surface Areas, Pore Volumes, And Rate Constants of Photodegradation of Methyl Orange of Three Representative Samples That Contain Two TiO_2 Shells

no.	sample	specific surface area (m^2/g)	pore volume (cm^3/g)	rate constant (min^{-1})
i	methyl orange (without catalyst)			0.0001
ii	SiO_2/TiO_2/PAN/ TiO_2	37.0	0.055	0.0006
iii	Hombikat UV 100	> 250		0.0016
iv	TiO_2/PAN/TiO_2	41.7	0.09	0.0020
v	TiO_2/TiO_2	34.2	0.099	0.0034

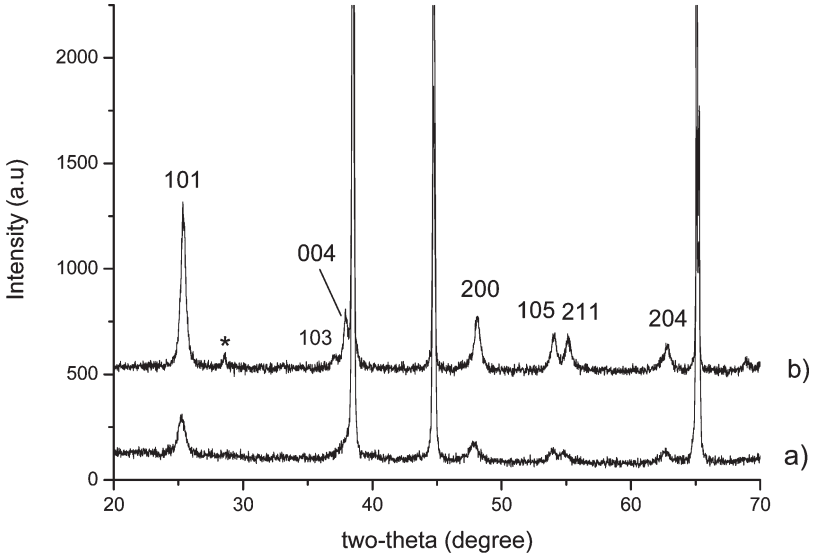

Figure 10. XRD patterns of (a): TiO_2/PANI/TiO_2 triple-shelled hollow spheres, and (b) double-shelled TiO_2 hollow spheres obtained after thermal removal of PAN interlayer phase; the large diffraction peaks belong to sample holder (Al). The peak (marked with an asterisk) belongs to metastable monoclinic TiO_2(B) after the thermal treatment.

TiF_4 prefers to form TiO_2 on the inner surface of TiO_2/PAN shell under similar synthetic parameters (Figures 1(vii) and Figure 8d; see the Supporting Information, SI-4). The observed growth preference is indeed another proof which shows that TiO_2 NPs were still left on the inner surface of PAN shell. The anatase nanoparticles residing inside the PAN shell serve once again as seeds for TiO_2 deposition, leading to a well-defined inner shell of TiO_2.

Under hydrothermal conditions, however, the TiF_4 hydrolysis becomes less selective and the TiO_2 can grow on both inner and outer surfaces of TiO_2/PAN hollow spheres, though the amount of the oxide on the inner surface is still slightly higher than that on the outer surface. This is due to more vigorous movement and interactions of reactants and templates under hydrothermal conditions, the difference between seeded and unseeded surfaces became less distinguishable. Figure 9a−d shows some examples of double-shelled TiO_2 hollow spheres (TiO_2/PAN/TiO_2; Figure 1(viii)) prepared with this hydrothermal method. Due to prevalence of thermodynamic control in hydrothermal reactions, anatase TiO_2 with high crystallinity can be obtained. After calcining the sample at 450 °C in laboratory air for 4 h, as shown in Figure 9e-f, PAN interlayer was completely burnt away, leaving double-shelled structures of anatase (i.e., TiO_2/TiO_2; Figure 1(ix)) behind. Our XRD investigation reported in Figure 10 confirms that both TiO_2/PAN/TiO_2 and TiO_2/TiO_2 hollow spheres have the tetragonal crystal structure (SG: $I4_1/amd$; JCPDS card no. 21−1272; a_o = 3.7852 Å and c_o = 9.5139 Å), noting that the latter sample shows sharper XRD peaks because of the additional heat-treatment at 450 °C.

In Figure 11, three representative samples that contain two TiO_2 shells in the shell structures are investigated for their surface area and porosity properties, and the analytical results are listed in Table 1 for reference. In all the cases, type H3 hysteresis loops are observed.[105] This type of hysteresis loops does not exhibit any limiting adsorption at high P/P^o region and is commonly attributed to particle aggregates with slit-shaped pores.[105] The pore-size distribution profiles across both microporous and mesoporous regions. In particular, the overlapping between adsorption and desorption curves is observed in the double-shelled hollow spheres of pure TiO_2. To compare their performance in actual applications, we have used these three samples for photocatalytic degradation of organic dyes under UV-light irradiation. In Figure 12, the photocatalytic reactivity of each sample is evaluated through the degradation of methyl orange, and the apparent rate constants according to a pseudo-first-order reaction with a simplified Langmuir−Hinshelwood model are also listed in Table 1.[106] Though the TiO_2/PAN/TiO_2 hollow spheres (Figure 9a−d) have the largest surface area 41.7 m^2/g among the three tested samples, it is nominally less active than the double-shelled TiO_2/TiO_2 (Figure 9e,f; 34.2 m^2/g). The surface area shrinkage of double-shelled hollow spheres is probably due to the heat treatment at 450 °C through which the internal mesopores merged. Although the SiO_2/TiO_2/PAN/TiO_2 core−shell nanocomposite (Figure 7a−c) gets a larger specific surface area (37.0 m^2/g) than the double-shelled anatase, its photocatalytic reactivity is the lowest due to presence of silica cores and PAN, and thus less TiO_2 content in the catalyst. Furthermore, the TiO_2 phase in the SiO_2/TiO_2/PAN/TiO_2 core−shell nanocomposite is less crystallized because of its low processing temperature (60 °C),

(105) Sing, K. S. W.; Everett, D. H.; Haul, R. A. W.; Moscou, L.; Pierotti, R. A.; Rouquerol, J.; Siemieniewska, T. *Pure Appl. Chem.* **1985**, *57*, 603–619.
(106) Wang, X. H.; Li, J.-G.; Kamiyama, H.; Moriyoshi, Y.; Ishigaki, T. *J. Phys. Chem. B* **2006**, *110*, 6804–6809.

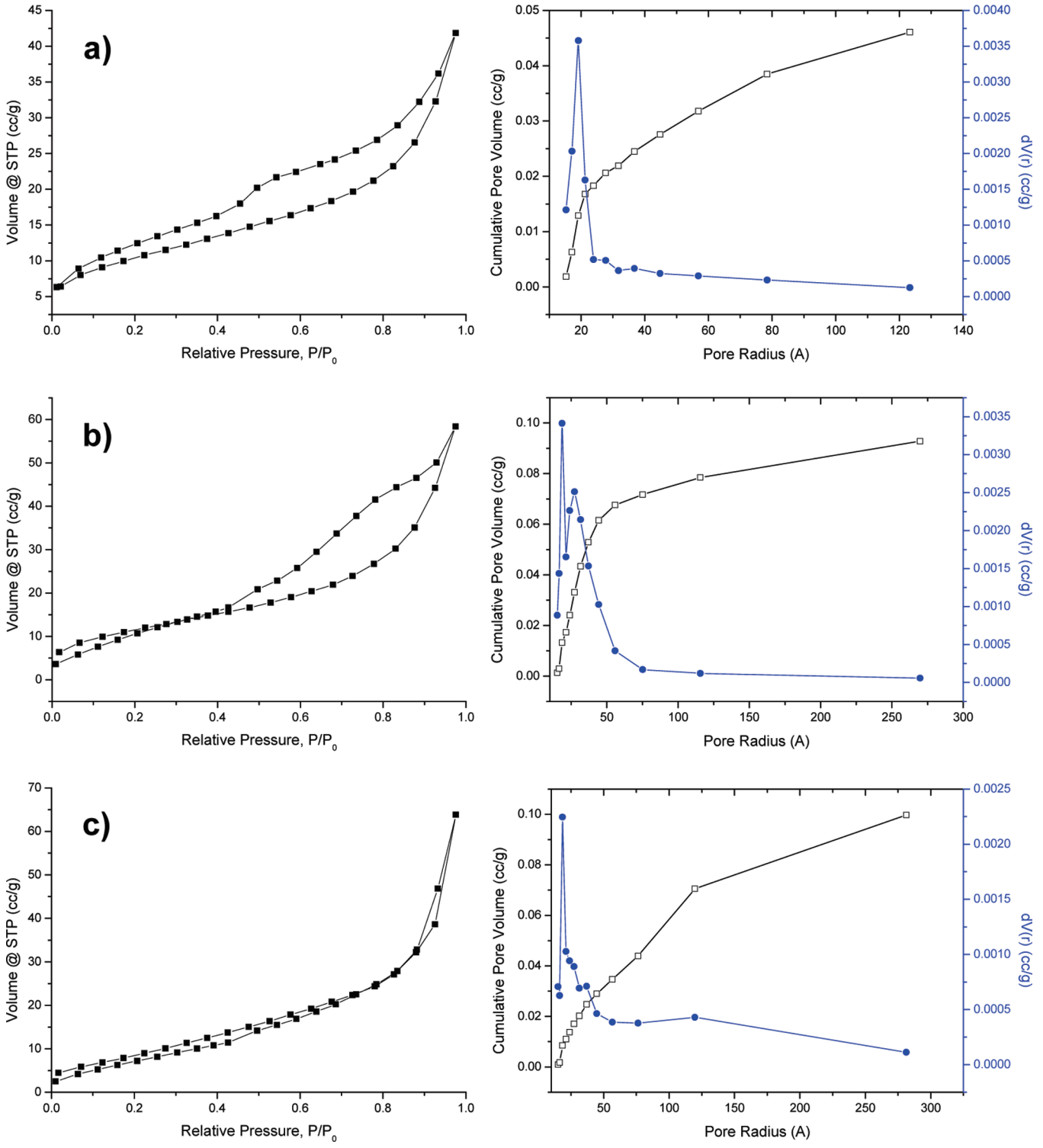

Figure 11. BET/BJH analyses of (a) $SiO_2/TiO_2/PAN/TiO_2$ core−shells, (b) $TiO_2/PAN/TiO_2$ triple-shelled hollow spheres, and (c) double-shelled TiO_2/TiO_2 hollow spheres.

compared with its hydrothermally and thermally treated counterparts in the same degradation study. Overall catalytic performance of the double-shelled TiO_2/TiO_2 hollow spheres is best among the all tested materials including Hombikat UV 100 as a reference. Using such complex shelled nanostructures can be advantageous for reactions in terms of easy separation and high reusability of catalysts after use, because of relatively large shell structures compared to normal unorganized nanoparticles. Considering their complex shell features and the presence of large interior space, nonetheless, we believe that these multishelled hollow spheres and the general nanoparticle-mediated synthetic approach developed in this work will become even more useful in the technological areas of membrane and intercalation applications where the requirements for pore-control and shell structures are more stringent. This challenging topic will be investigated in our future research.

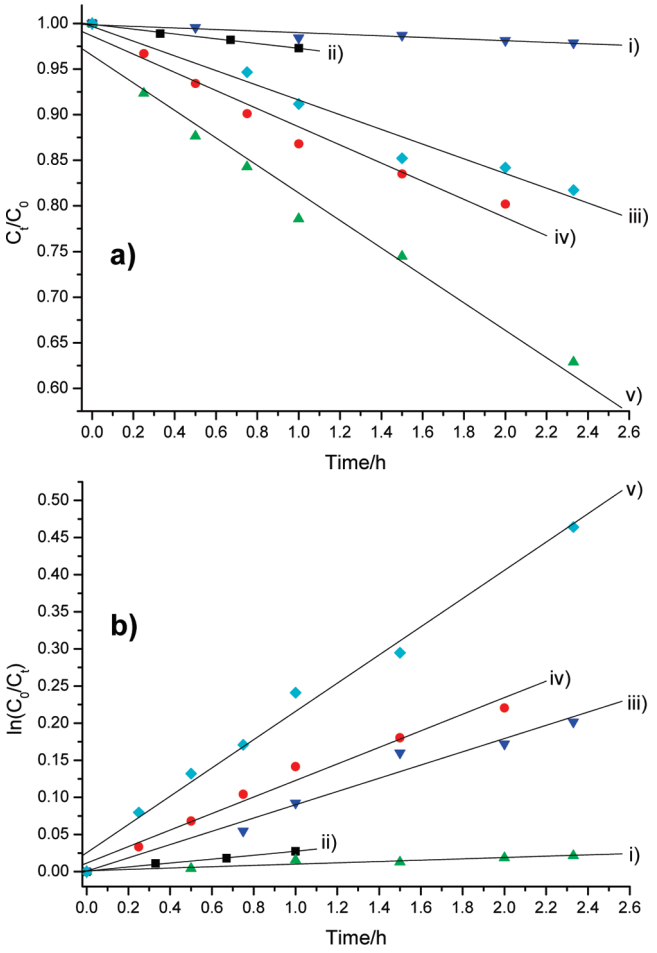

Figure 12. C_t/C_o-versus-time plots (a) and $\ln(C_t/C_o)$-versus-time plots (b) for: (i) methyl orange solution (i.e., without solid catalyst), (ii) $SiO_2/TiO_2/PAN/TiO_2$ core−shells, (iii) Hombikat UV 100, (iv) triple-shelled $TiO_2/PAN/TiO_2$ hollow spheres, and (v) double-shelled TiO_2/TiO_2 hollow spheres.

4. Conclusions

In summary, through exploring multifunctional roles of anatase TiO_2 nanoparticles, we have developed several solution-based chemical schemes to prepare core−shell and hollow-sphere nanocomposites comprising sol−gel-derived silica, anatase TiO_2 and polyaniline. More specifically, we have devised a nanoparticle-mediated approach for preparation of complex core−shell and hollow sphere nanostructures, in which oleate-surfactant-protected anatase TiO_2 nanoparticles play multifunctional roles in the construction of highly complex nanostructures: as starting sites for deposition of polyaniline shell on SiO_2 mesospheres; as a secondary material phase anchored on the inner surface of polyaniline shell; as preinstalled seeds for homogeneous growth of TiO_2 inner shell on the polyaniline; and as primary nanobuilding blocks to prepare external oxide shell on the polyaniline via self-assembly. With the assistance of the TiO_2 nanoparticles, the present approach has shown high synthetic flexibility for tailor-making complex shelled nanostructures with different architectural designs. A total of six types of composite structures have been fabricated with this approach, namely, core−shells of SiO_2/TiO_2, $SiO_2/TiO_2/PAN$, and $SiO_2/TiO_2/PAN/TiO_2$, and complex hollow spheres of TiO_2/PAN, $TiO_2/PAN/TiO_2$, and TiO_2/TiO_2. Our preliminary experimental result also shows the applicability of these nanostructures in real photocatalytic applications, especially for the separation of used catalysts after reaction owing to their relatively large external diameters. Because other size-defined metal-oxide nanoparticles can also be facilely prefabricated nowadays and the main process steps involved in this type of approach are well separate and relatively simple (e.g., self-assembly, templating growth, polymerization, homogeneous seeded growth, etc.), we believe that the current architectural design and synthetic approach can be easily extended to other complex polymer−metal-oxide systems.

Acknowledgment. The authors gratefully acknowledge the Economic Development Board, Singapore, and King Abdullah University of Science and Technology, Saudi Arabia, for support of this research. D.P.W. also thanks the National University of Singapore for providing her postgraduate scholarship.

Supporting Information Available: Additional figures (PDF). This material is available free of charge via the Internet at http://pubs.acs.org.